Supporting information for

Construction of highly durable electrocatalysts by pore-confinement and anchoring effect for oxygen reduction reaction

Anyong Chen [a,b,†], Jiajia Lu [a,†], Hongwei Zhu [a], Hongxia Zhang [a], Shaojuan Zeng [e], Lirong Zheng [c,*], Han-Pu Liang [a,b,d,*]

[a] Qingdao Institute of Bioenergy and Bioprocess Technology, Chinese Academy of Sciences, Qingdao 266101, China

[b] Center of Materials Science and Optoelectronics Engineering, University of Chinese Academy of Sciences, Beijing 100049, China

[c] Beijing Synchrotron Radiation Facility, Institute of High Energy Physics, Chinese Academy of Sciences, Beijing 100049, China

[d] Dalian National Laboratory for Clean Energy, Chinese Academy of Sciences, Dalian 116023, China

[e] Institute of Process Engineering, Chinese Academy of Sciences, Beijing 100190, China

* Corresponding Authors E-mails: zhenglr@ihep.ac.cn (L. Zheng); lianghp@qibebt.ac.cn (H-P. Liang)

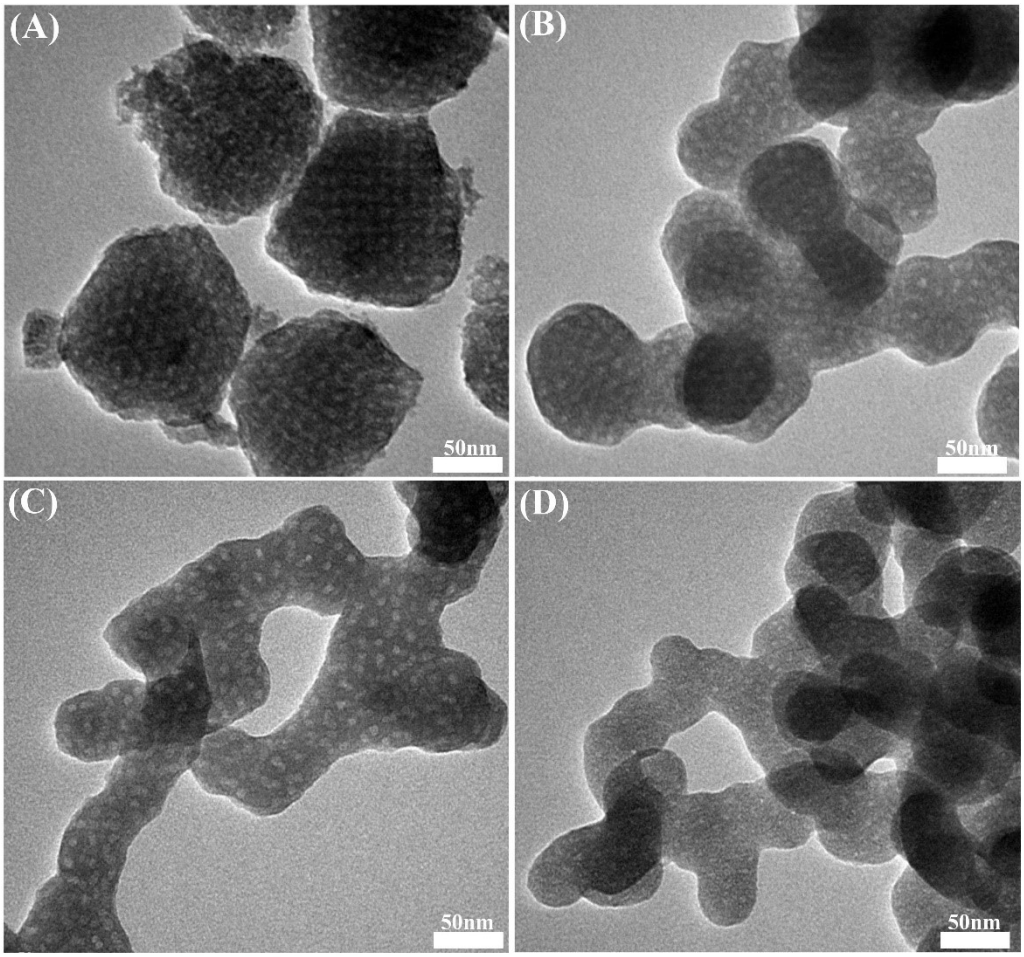

Figure S1. TEM images of porous carbon (PC) precursor with various amount of phytic acid (PA): (A) 0 ml (B) 0.1 ml (C) 0.2 ml and (D) 0.3 ml.

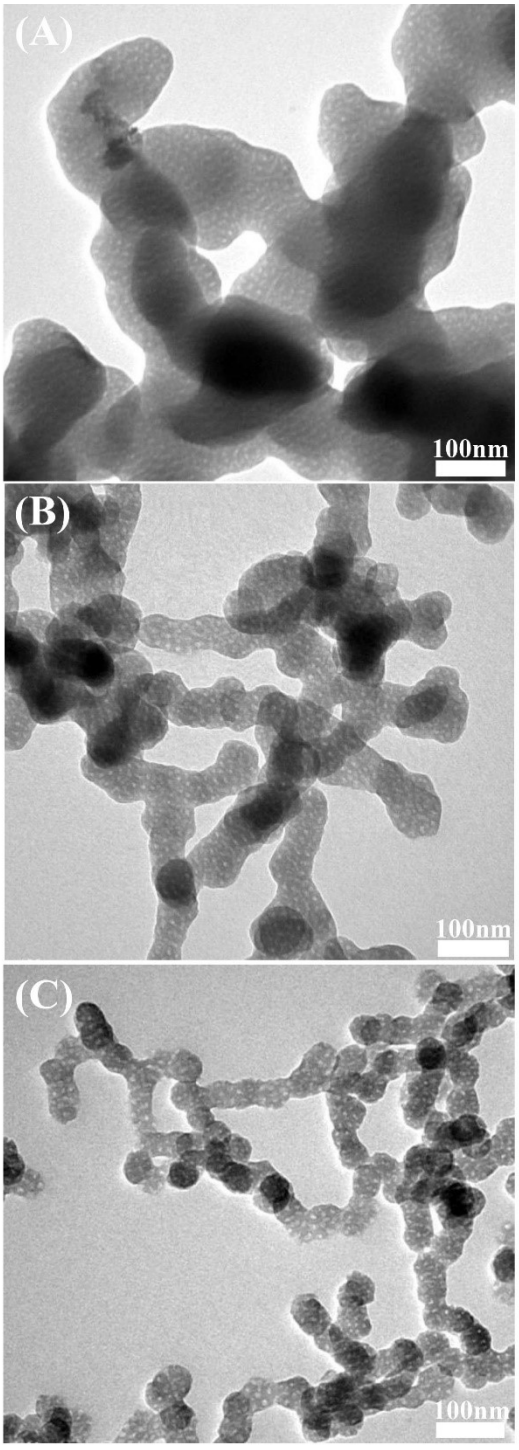

Figure S2. TEM images of PC precursor composite with various amount of F127: (A) 1 g (B) 1.5 g and (C) 2 g.

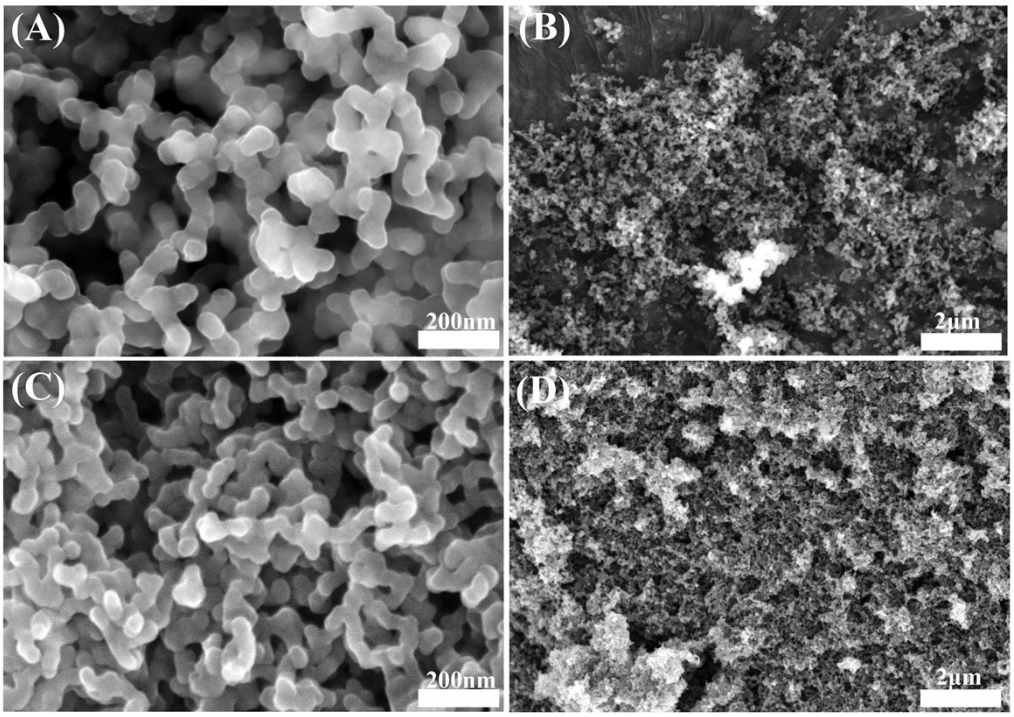

Figure S3. SEM images of (A, B) PC precursor and (C, D) PC.

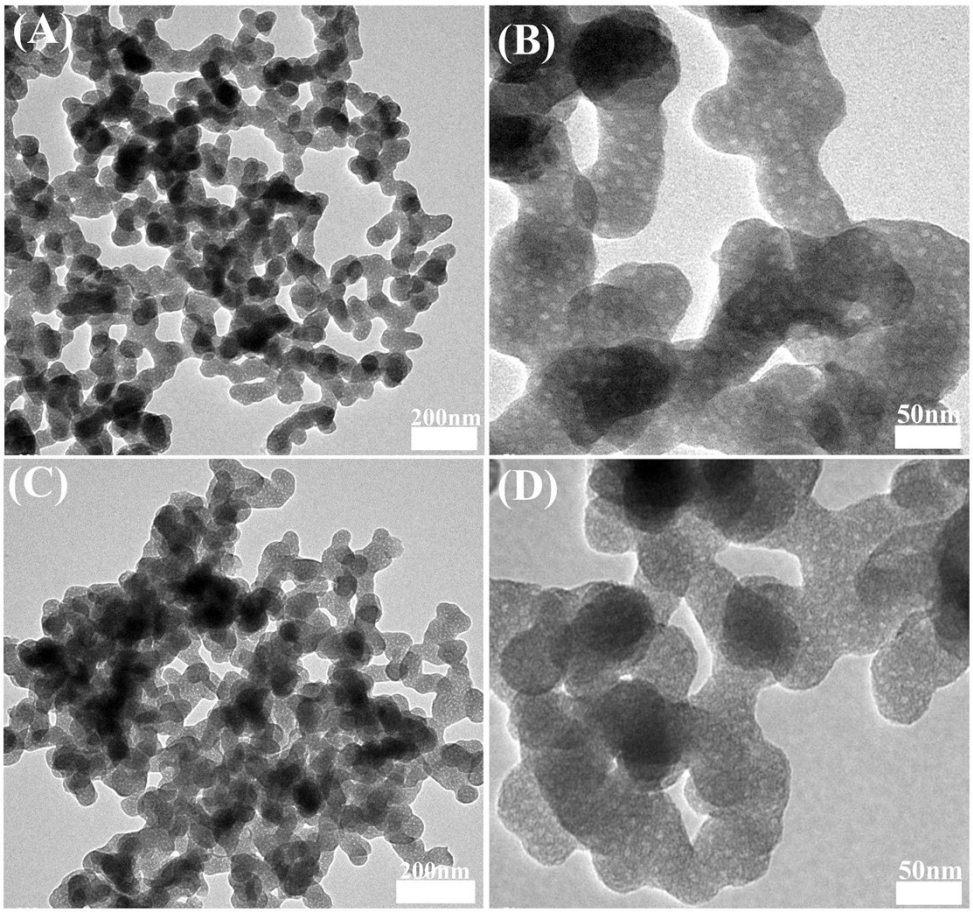

Figure S4. TEM images of (A, B) PC precursor, (C, D) PC.

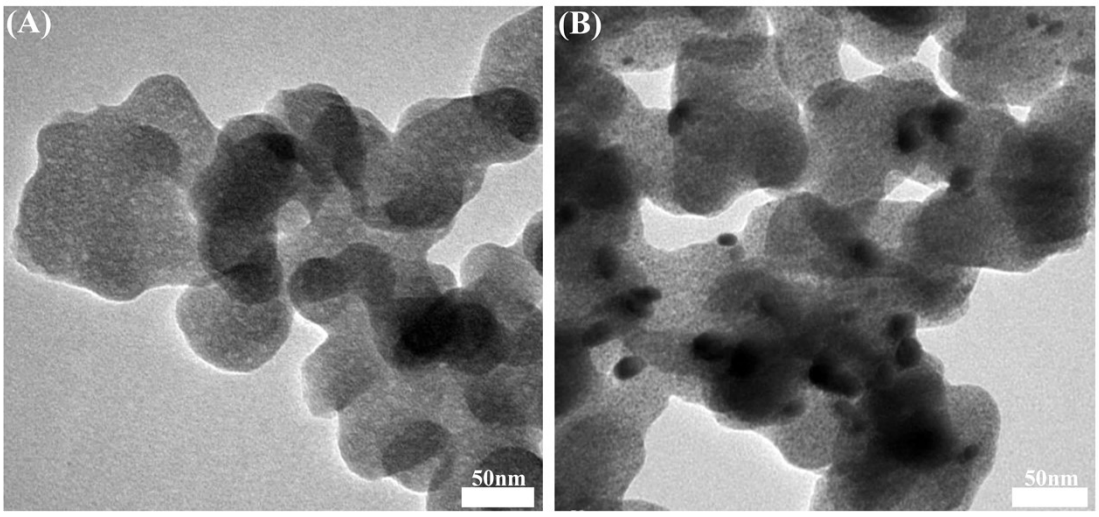

Figure S5. TEM images of (A) Pt-PC-200, (B) Pt-PC-400.

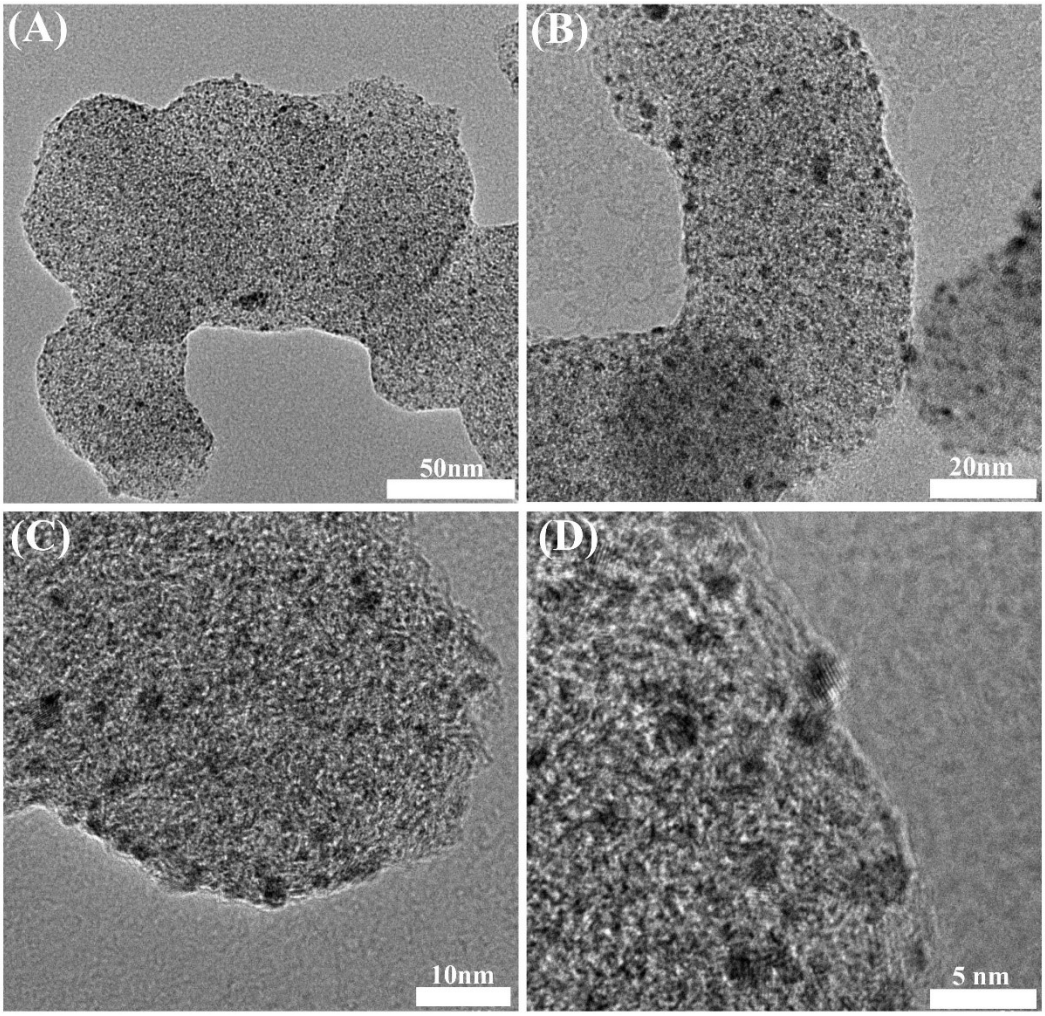

Figure S6. HRTEM images of the Pt-PC-300.

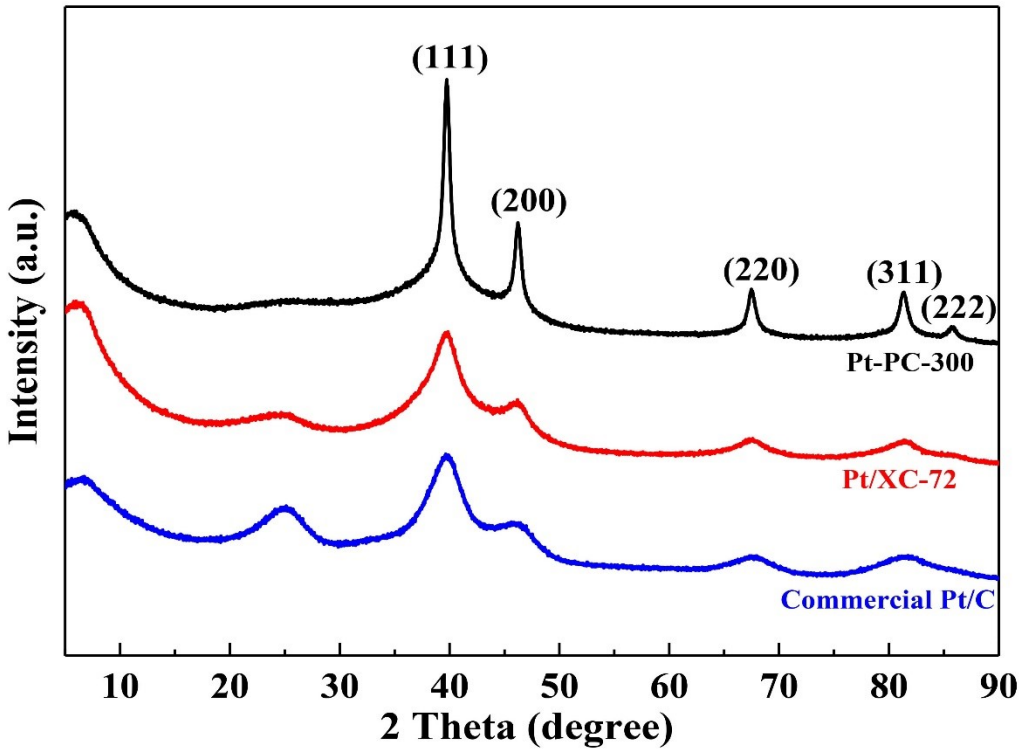

Figure S7. XRD patterns of Pt-PC-300, Pt/XC-72 and commercial Pt/C.

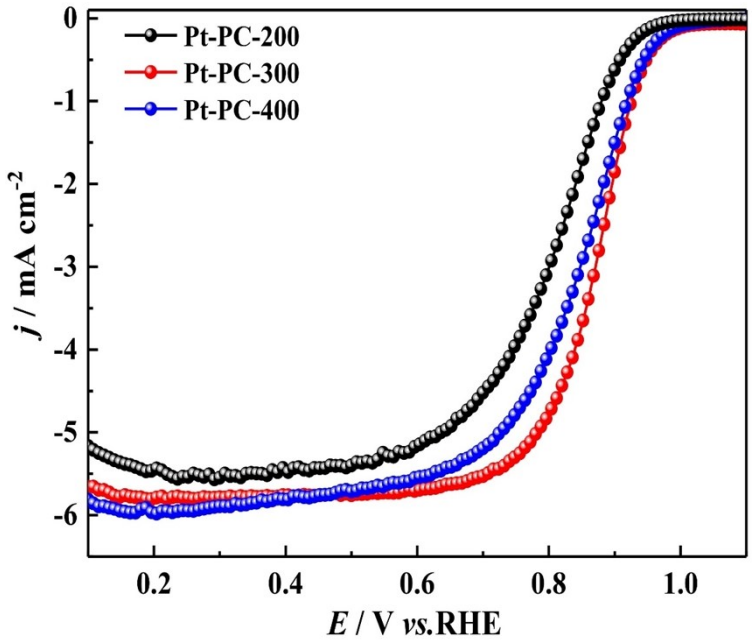

Figure S8. LSV curves of Pt-PC-200, Pt-PC-300 and Pt-PC-400 in 0.1 M $HClO_4$ aqueous solution.

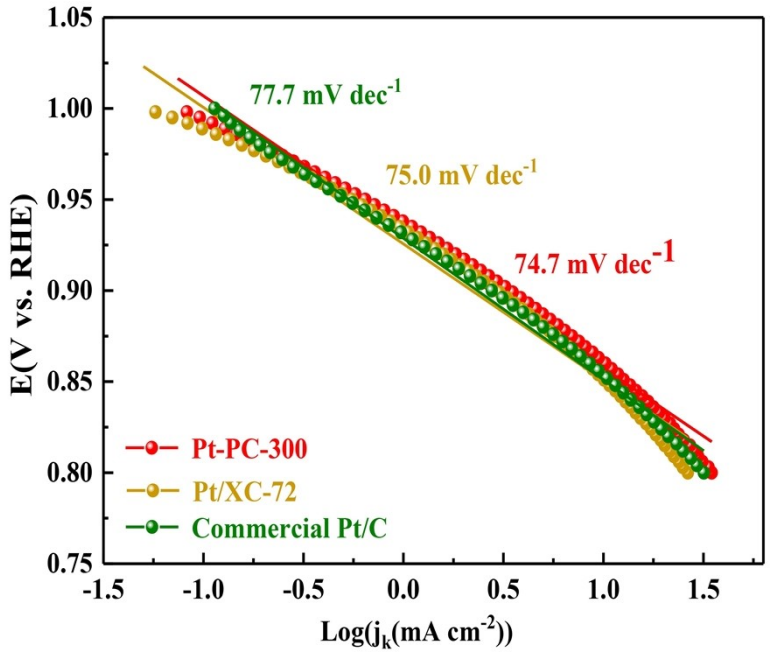

Figure S9. Tafel plots of Pt-PC-300, Pt/XC-72 and commercial Pt/C.

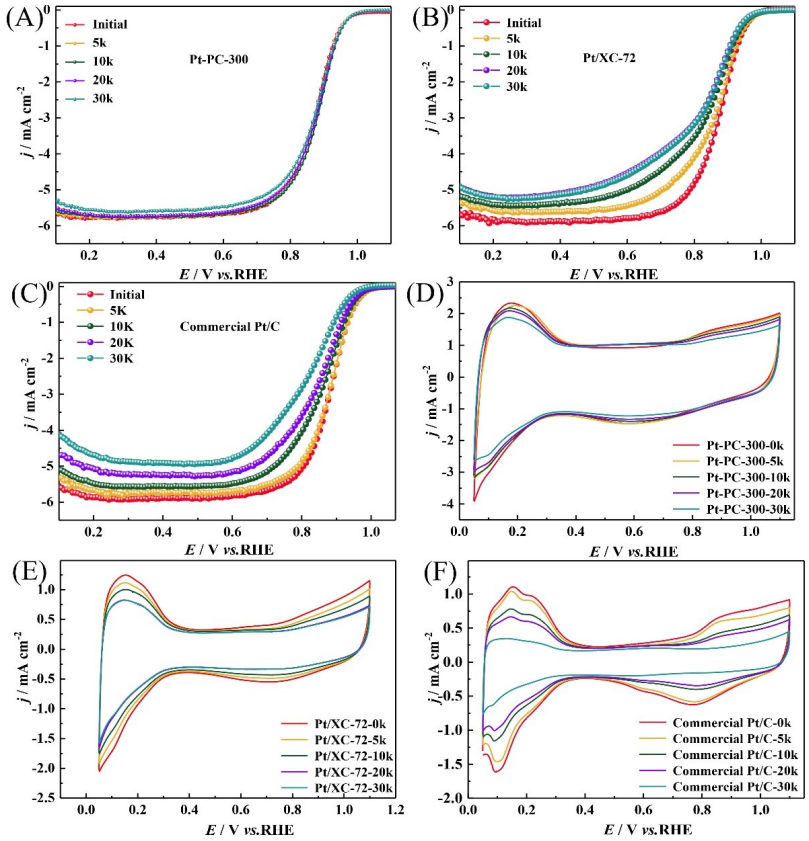

Figure S10. (A-C) LSV curves of Pt-PC-300, Pt/XC-72 and commercial Pt/C in O_2-saturated 0.1 M $HClO_4$ aqueous solution at different cycles. (D-F) The corresponding CV curves for the prepared catalysts in N_2-saturated 0.1 M $HClO_4$ aqueous solution.

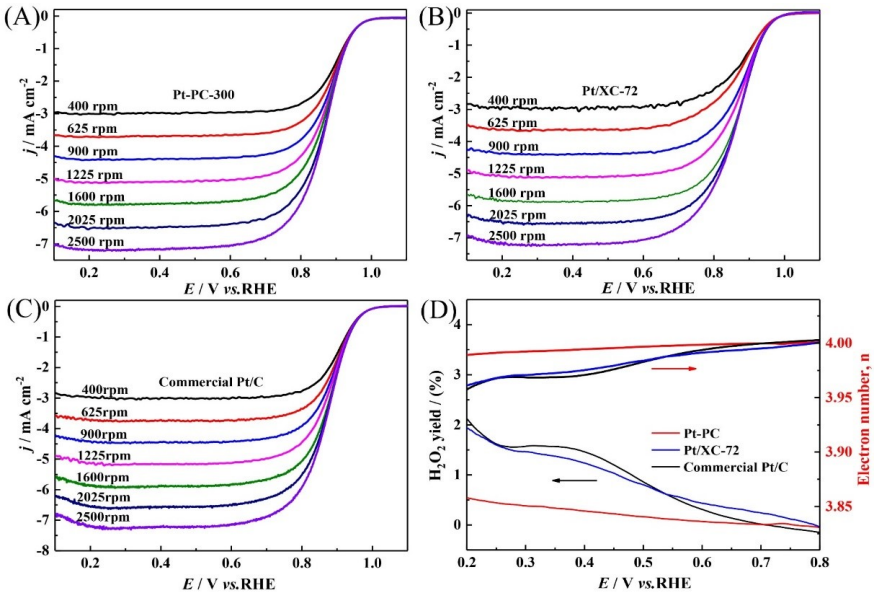

Figure S11. LSV curves of (A) Pt-PC-300, (B) Pt/XC-72 and (C) commercial Pt/C at different rotation speeds. (D) Corresponding electron transfer number (n) and H_2O_2 yield of Pt-PC-300, Pt/XC-72 and commercial Pt/C.

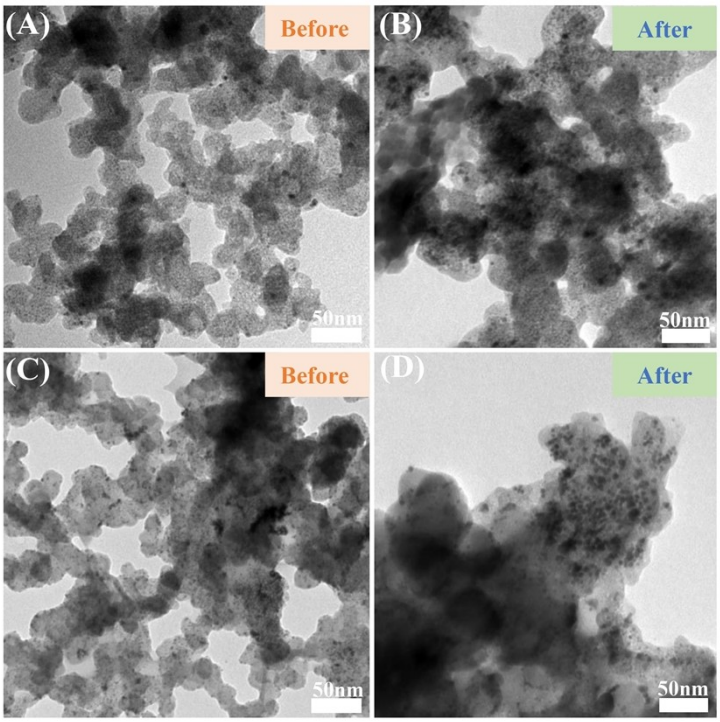

Figure S12. TEM images of (A, B) Pt/XC-72 and (C, D) commercial Pt/C before and after stability testing.

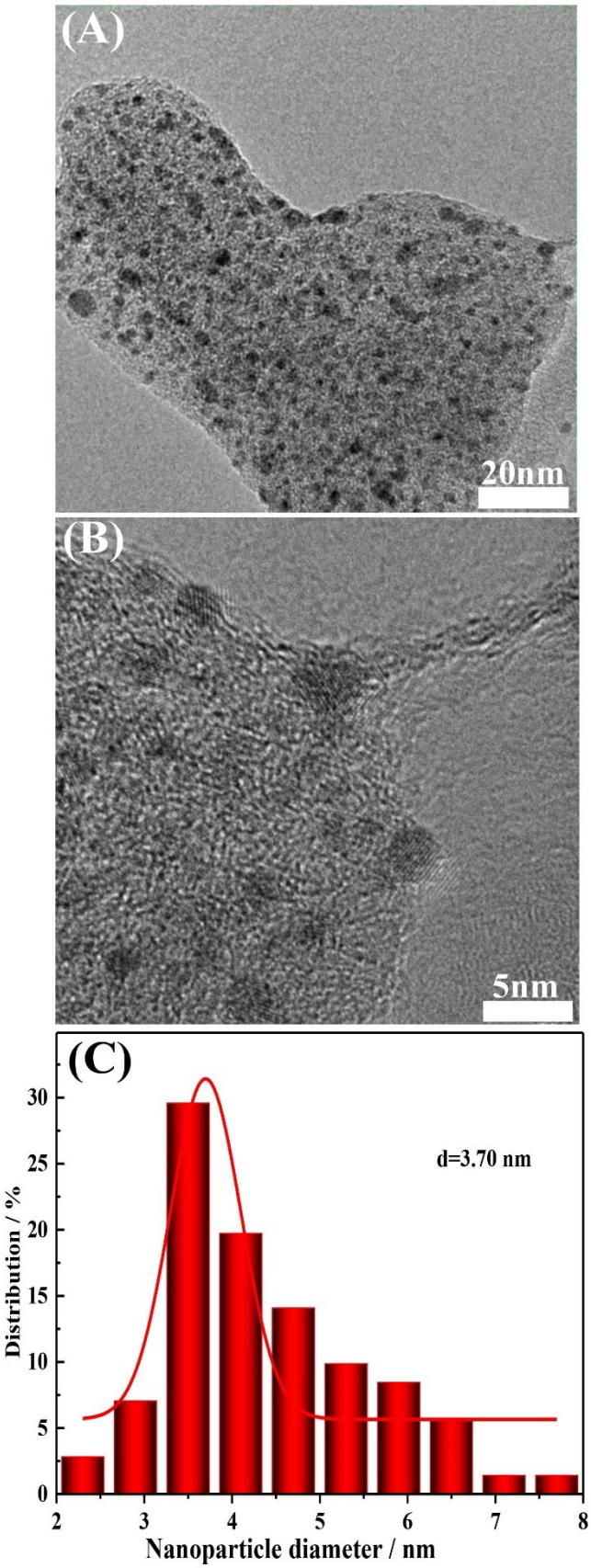

Figure S13. (A, B) HRTEM images and (C) the corresponding particle size distribution of Pt-PC-300 after stability testing.

Table S1. The contents of C, N, O, P and Pt in Pt-PC-300 from XPS.

Element	C	N	O	P	Pt
Content (at %)	82.17	3.68	9.74	0.66	3.75

Table S2. EXAFS fitting parameters at the Pt L_3-edge for various samples.

Sample	Shell	N [a]	R (Å) [b]	σ^2 (Å$^2\cdot10^{-3}$) [c]	ΔE_0 (eV) [d]	*R* factor (%)
Pt-PC-300	Pt-O	2.8	2.02	5.6	11.1	0.9
	Pt-Pt	2.6	2.78	5.9	14.7	

a) N: coordination numbers; b) R: bond distance; c) σ^2: Debye-Waller factors; d) ΔE_0: the inner potential correction. e) R factor: goodness of fit. f) S_0^2 were set as 0.84/0.90 for Pt-O/Pt-Pt, which were obtained from the experimental EXAFS fit of reference PtO_2/Pt foil by fixing CN as the known crystallographic value and was fixed to all the samples[1-3].

Table S3. The initial $E_{1/2}$ (V) of Pt-PC-300 at different temperature.

Catalysts	Pt-PC-200	Pt-PC-300	Pt-PC-400
$E_{1/2}$ (V)	0.802	0.871	0.848

Table S4. Comparison of $E_{1/2}$ (V) among different catalysts in 0.1 M $HClO_4$.

Catalysts	Initial	5k	10k	20k	30k	After 30k
Pt/XC-72	0.872	0.859	0.835	0.812	0.813	-0.059
Commercial Pt/C	0.880	0.878	0.853	0.834	0.787	-0.093
Pt-PC-300	0.871	0.874	0.881	0.876	0.877	+0.006

Table S5. Comparison of Mass Activity (mA mg_{Pt}^{-1}) of the synthesized catalysts.

Catalysts	Initial	5k	10k	20k	30k	Change (%)
Pt/XC-72	114.92	84.4	70.27	58.02	60.34	-47.5
Commercial Pt/C	113.56	112.94	59.50	59.27	34.12	-67.0
Pt-PC-300	107.29	112.80	142.91	130.93	120.77	+12.6

Table S6. Comparison of ECSA (m^2 g^{-1}) of the synthesized catalysts at different cycles.

Catalysts	Initial	5k	10k	20k	30k	Change (%)
Pt/XC-72	53.23	46.65	41.56	32.64	31.52	-40.8
Commercial Pt/C	52.58	48.53	34.19	28.81	10.32	-80.4
Pt-PC-300	80.40	69.86	65.67	60.48	50.77	-36.9

Table S7. Mass activity, ECSA and Tafel slops of Pt-PC-300 for ORR in this work and several results of representative Pt based catalysts from recent published work.

Catalysts	$E_{1/2}$ (V)	Pt loading (μg_{Pt} cm^{-2})	Mass activity ($mAmg_{Pt}^{-1}$) (0.9V)	The retention rate of MA (30k)	ECSA (m^2/g) (0.9V)	Tafel slops ($mV\ dec^{-1}$)	Ref
Pt/MWCNT	0.862	50	58.8	52.38%	56.4	70	[4]
Pt/MU-MWCNT	0.915	50	174.5	63.32%	103.4	63	[4]
Pt/C-JM	0.89	50	92.4	96.96%	77.8	63	[4]
Pt-TNT/FAB	0.79	20	37.5	-	49.6	64	[5]
Pt NAs	0.839	200	12.4(0.85V)	-	47.7(0.85V)	-	[6]
Pt/NS-Ti_4O_7	-	96	22.33(0.85V)	59.61%(3k)	58.7(0.85V)	-	[7]
Pt/RGO_1-FCB_2	0.886	180	249	-	62.1	-	[8]
Pt-Ni/ graphene	0.77	40	0.14(0.8V)	-	0.31(0.8V)	-	[9]
Pt nanoplates	0.847	-	449	82.1%(5k)	25.6	-	[10]
Pt-PC-300	0.881	25.4	142.91	112.6%	80.40	74.7	This work

References

[1] Ravel, B.; Newville, M. ATHENA, ARTEMIS, HEPHAESTUS: data analysis for X-ray absorption spectroscopy using IFEFFIT. Journal of synchrotron radiation 12 (2005) 537-541 https://doi.org/10.1107/s0909049505012719.

[2] Bouwens, S. M. A. M.; Koningsberger, D. C.; de Beer, V. H. J.; Prins, R. The structure of the cobalt sulfide phase in carbon-supported co and co-mo sulfide catalysts as studied by exafs and xanes. Catalysis Letters 1 (1988) 55-59 https://doi.org/10.1007/bf00765354.

[3] Rehr, J. J.; Albers, R. C. Theoretical approaches to x-ray absorption fine structure. Reviews of Modern Physics 72 (2000) 621-654 https://doi.org/10.1103/RevModPhys.72.621.

[4] Shu, Q. Z.; Xia, Z. X.; Wei, W.; Xu, X. L.; Sun, R. L.; Deng, R. Y.; Yang, Q. H.; Zhao, H.; Wang, S. L.; Sun, G. Q. Controllable Unzipping of Carbon Nanotubes as Advanced Pt Catalyst Supports for Oxygen Reduction. Acs Applied Energy Materials 2 (2019) 5446-5455 https://doi.org/10.1021/acsaem.9b00506.

[5] Bukka, S.; Badam, R.; Vedarajan, R.; Matsumi, N. Photo-generation of ultra-small Pt nanoparticles on carbon-titanium dioxide nanotube composites: A novel strategy for efficient ORR activity with low Pt content. International Journal of Hydrogen Energy 44 (2019) 4745-4753 https://doi.org/10.1016/j.ijhydene.2019.01.004.

[6] Xia, B. Y.; Ng, W. T.; Wu, H. B.; Wang, X.; Lou, X. W. D. Self-Supported Interconnected Pt Nanoassemblies as Highly Stable Electrocatalysts for Low-Temperature Fuel Cells. Angewandte Chemie 124 (2012) 7325-7328 https://doi.org/10.1002/ange.201201553.

[7] Yao, C. H.; Li, F.; Li, X.; Xia, D. G. Fiber-like nanostructured Ti_4O_7 used as durable fuel cell catalyst support in oxygen reduction catalysis. Journal of Materials Chemistry 22 (2012) 16560-16565 https://doi.org/10.1039/c2jm32866f.

[8] Tang, X. J.; Zeng, Y. C.; Cao, L. S.; Yang, L. M.; Wang, Z. Q.; Fang, D. H.; Gao, Y. Y.; Shao, Z. G.; Yi, B. L. Anchoring ultrafine Pt nanoparticles on the 3D hierarchical self-assembly of graphene/functionalized carbon black as a highly efficient oxygen reduction catalyst for PEMFCs. Journal of Materials Chemistry A 6 (2018) 15074-15082 https://doi.org/10.1039/c8ta02453g.

[9] Suh, W. K.; Ganesan, P.; Son, B.; Kim, H.; Shanmugam, S. Graphene supported Pt-Ni nanoparticles for oxygen reduction reaction in acidic electrolyte. International Journal of Hydrogen Energy 41 (2016) 12983-12994 https://doi.org/10.1016/j.ijhydene.2016.04.090.

[10] Nakamoto, T.; Motomiya, K. I.; Yokoyama, S.; Takahashi, H. Precursor-templated synthesis of thermodynamically unfavored platinum nanoplates for the oxygen reduction reaction. Dalton transactions 49 (2020) 15837-15842 https://doi.org/10.1039/d0dt03338c.